Disk Element Model for Simulation of Failure Behavior of Concrete under Biaxial Stresses

Mostafa A. M. ABDEEN* and Tatsuya TSUBAKI**

*M.S., Graduate Student, Dept. of Civil Engineering, Yokohama National University, Hodogaya-ku, Yokohama 240

**Ph.D., Associate Professor, Dept. of Civil Engineering, Yokohama National University

Numerical simulations have great advantages in investigating the failure mechanism of brittle composite materials such as concrete because the motion of each individual element and the internal mechanical state of each contact can be followed. In the present study, a numerical model is investigated to simulate the failure behavior of concrete under biaxial stresses using two-dimensional disk elements taking into account the degradation of material stiffness at the contact line. The stress-strain relationship and the volume change process up to the global failure are simulated by using the present model. Also, the internal crack formation is simulated to investigate the failure mechanism of concrete. The failure surface envelope of model concrete under biaxial stresses is obtained from simulation results. Good agreement is obtained between the numerical results and the experimental data.

Key Words : *disk element model, material modeling, simulation, concrete*

1. INTRODUCTION

Methods for material failure analysis are divisible into two main categories. The first category including ordinary finite element and boundary element methods can be applied to problems in which the material is regarded as continuum, but difficulties arise if the material becomes separated by cracking after tensile failure. The second category including distinct element and interface element methods can be used before and after failure continuously. The distinct element method (DEM) was introduced by Cundall to analyze a granular assembly numerically. The first model[1] used two-dimensional polygonal elements and the second model[2] used circular elements to reduce the complexity of modeling and the computational time. The interface element method was introduced by Zubelewicz and Bažant[3] modifying the DEM by considering the brittle aggregate composite as a system of perfectly rigid particles separated by interface layers. The lattice model was introduced by Schlangen and Mier[4] and the microstructural unit element method, by Tsubaki[5]. These models are used at a small scale, where the small structural elements of concrete are generated and aggregate, matrix and interface properties are assigned to each element. In this research circular disk elements are used to investigate a numerical method able to simulate the macroscopic failure behavior of concrete using the assumed mesoscopic material model.

2. DISK ELEMENT MODEL

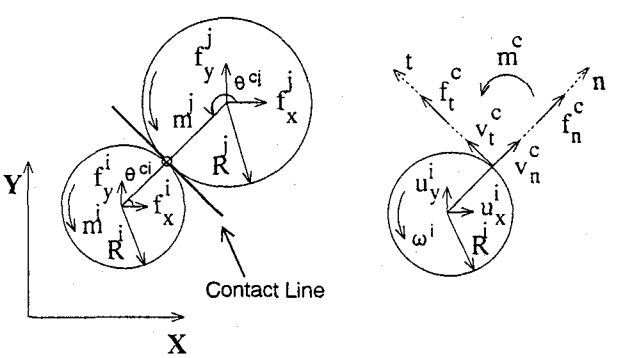

Figure 1 Disk Element Model

Fig.1 shows two disk elements in contact with each other. In Fig.1, X,Y are the global coordinate axes, and n,t are the local coordinate axes defined at the center of the contact line. A contact line is located at the contact point or between two disk elements and its length is equal

to the average of the diameters of the two disk elements.

The relative normal and tangential displacements and rotation of element j with respect to element i at the center of the contact line (v_n^c, v_t^c, ω^c) are obtained as follows:

$$\boldsymbol{V}^c = -\boldsymbol{T}^{cj}\boldsymbol{U}^j - \boldsymbol{T}^{ci}\boldsymbol{U}^i; \quad \boldsymbol{V}^c = [v_n^c, v_t^c, \omega^c]^T; \quad \boldsymbol{U}^i = [u_x^i, u_y^i, \omega^i]^T;$$

$$\boldsymbol{T}^{ci} = \begin{bmatrix} cos\theta^{ci} & sin\theta^{ci} & 0 \\ -sin\theta^{ci} & cos\theta^{ci} & R^i \\ 0 & 0 & 1.0 \end{bmatrix} \qquad (1)$$

where $\boldsymbol{V}^c$ is the relative displacement vector for the center of the contact line, $\boldsymbol{T}^{ci}$ is the transformation matrix needed to transform the global quantities of element i to the local quantities at the center of the contact line, and $\boldsymbol{U}^i$ is the global displacement vector for the centroid of element i. Superscript c indicates a quantity related to the center of a contact line.

The local contact forces and moment at the contact line (f_n^c, f_t^c, m^c) are obtained by applying the force displacement relationship as follows:

$$\boldsymbol{F}^c = \boldsymbol{K}^c\boldsymbol{V}^c; \quad \boldsymbol{F}^c = [f_n^c, f_t^c, m^c]^T;$$

$$\boldsymbol{K}^c = \begin{bmatrix} k_n^c & 0 & 0 \\ 0 & k_t^c & 0 \\ 0 & 0 & k_m^c \end{bmatrix} \qquad (2)$$

where $\boldsymbol{F}^c$ is the local contact force vector for the center of the contact line, $\boldsymbol{K}^c$ is the stiffness matrix of the contact line, and k_n^c, k_t^c and k_m^c are the normal, tangential and rotational stiffnesses calculated from the stiffnesses of the contact line.

Then the equilibrium equation for element i is expressed as follows:

$$\boldsymbol{F}^i = \sum_{j=1}^{n} \boldsymbol{T}^{ciT}\boldsymbol{F}^c; \quad \boldsymbol{F}^i = [f_x^i, f_y^i, m^i]^T \qquad (3)$$

where n is the number of elements which are in contact with element i, $\boldsymbol{F}^i$ is the external global force vector of element i, and f_x^i, f_y^i, m^i are the external global forces and moment acting at the centroid of element i. Eq.3 is made for every element in sequence and assembled to get the global equilibrium equation to be solved to obtain the global displacement vector for all the elements of the structure.

The reactions of the elements can be obtained by the following equation.

$$\boldsymbol{R} = \boldsymbol{K}\boldsymbol{U} \qquad (4)$$

where $\boldsymbol{R}$ is the global reaction vector for all the elements in sequence, $\boldsymbol{K}$ is the global stiffness matrix for the structure, and $\boldsymbol{U}$ is the global displacement vector for all the elements in sequence.

3. MATERIAL MODELING

3.1 Stress-strain relationship

Fig.2 illustrates the stress-strain relatioship for the material of the contact line. It is assumed that material behavior of the contact line is elastic up to the peak. In tension it is assumed to be brittle but in compression and shear ductile models are used after reaching each strength.

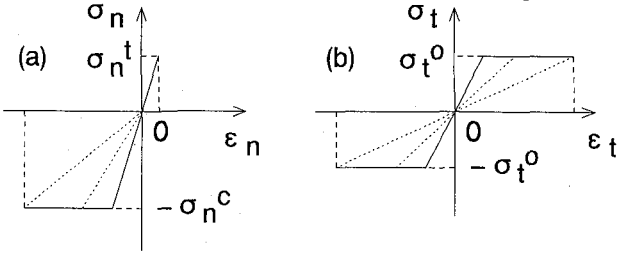

Figure 2 Stress-Strain Diagram for Material of Contact Line
(a) Normal Direction ; (b) Tangential Direction

3.2 Failure criteria

The maximum stress failure criterion is used for the behavior in the normal and tangential directions independently. In the case of tension the contact line fails when the stress reaches the tensile strength σ_n^t. In the cases of compression and shear the contact line fails when the stress reaches the compressive strength σ_n^c or the shear strength σ_t^o, and each stiffness is reduced to give some ductility to the material of the contact line.

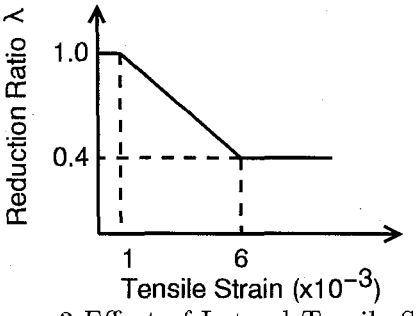

Figure 3 Effect of Lateral Tensile Strain on Compressive Strength

A strength reduction law is used together with the maximum stress failure criterion in the loading of combined compression and tension where the compressive strength of the contact line is reduced as a function of the lateral tensile strain using a relationship similar to that introduced by

Vecchio and Collins[6]. Fig.3 shows the reduction ratio as a function of the lateral tensile strain. The same reduction ratio is used for the adjacent diagonal contact lines for simplicity. This reduction law accounts for the effect of significant tensile cracking and formation of continuous cracks in the early stage.

3.3 Gradual degradation model

The gradual degradation law is used for compression and shear for which the stiffness is reduced to 50% of the current value every time when the stress of the contact line reaches the strength.The number of degradations n_d is specified and the stiffness becomes zero after n_d is reached. This gradual degradation law is essential to model the behavior of the mesoscopic structure of concrete.

4. CONTACT LINE MODEL

The contact line is divided into several layers for tension and compression as shown in Fig.4 and failure criteria are examined at each layer. The normal, tangential and rotational stiffnesses can be calculated as follows.

$$k_n^c = \frac{1}{H^c}\int_{A^c} E^c\, dA^c = \frac{1}{H^c}\sum_{i=1}^{n_l} E_i^c A_i^c \qquad (5)$$

$$k_t^c = \frac{G^c A_t^c}{H^c} \qquad (6)$$

$$k_m^c = \int_{A^c} E^c \xi^2\, dA^c = \sum_{i=1}^{n_l} E_i^c \xi_i^2 A_i^c \qquad (7)$$

where E^c, G^c and H^c are the elastic modulus, shear regidity and the distance between the centroids of the elements respectively. A^c is the area of contact line, and A_t^c, the area for shear resistance, being equal to A^c. The height of A^c is equal to $R^i + R^j$ and the width is taken equal to unity. It is assumed that the contact line fails when 60% of layers fail in tension. In case of compression the maximum stress is used for failure check.

The normal and tangential stresses, σ_n, σ_t, at the contact line are calculated by the following equations.

$$\sigma_n = \frac{f_n^c}{A^c} + \frac{m^c \xi}{I^c};\quad \sigma_t = \frac{f_t^c}{A_t^c} \qquad (8)$$

where I^c is the second moment of inertia of the contact line around the center of rotation the position of which is fixed and f_t^c is the shear force.

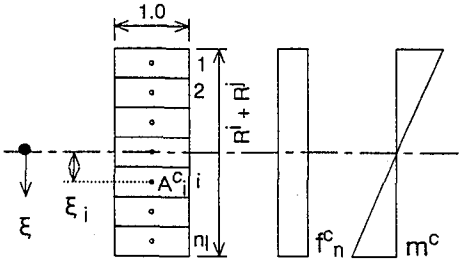

Figure 4 Layered Contact Line with Normal Stress Distribution by Normal Force and Moment

5. NUMERICAL ANALYSIS PROCEDURE

The numerical simulation is done by using the secant method to assure the numerical stability. It is assumed that the deformation is small and the position of contact line is not updated in each loading step. The flow of the analysis is summarized in a flow chart as shown in Fig.5.

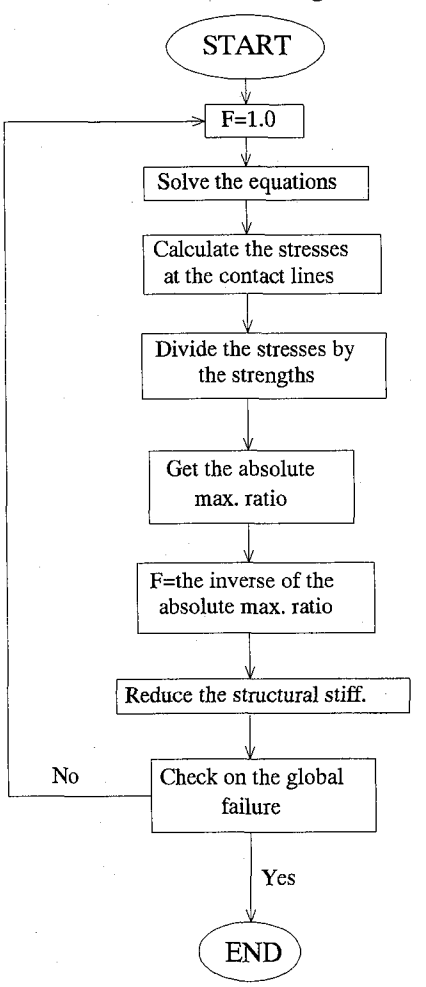

Figure 5 Flow of Analysis Using Secant Method

The analysis procedure is summarized as follows.

1. Apply unit force in the direction of the load.
2. Solve the equilibrium equations for all the elements.
3. Calculate the normal and shear stresses at the contact lines.
4. Divide all these stresses by the corresponding strength in the normal and tangential directions of contact lines.
5. Get the absolute maximum value among all the stress ratios.
6. Calculate the inverse of this absolute maximum value as the imposed force to get a failure at only one contact line.
7. Reduce the structural stiffness according to the position of the contact line which reaches the failure.
8. Repeat all these steps until the global failure which is determined according to the excessively large value of the displacement.

6. NUMERICAL SIMULATION

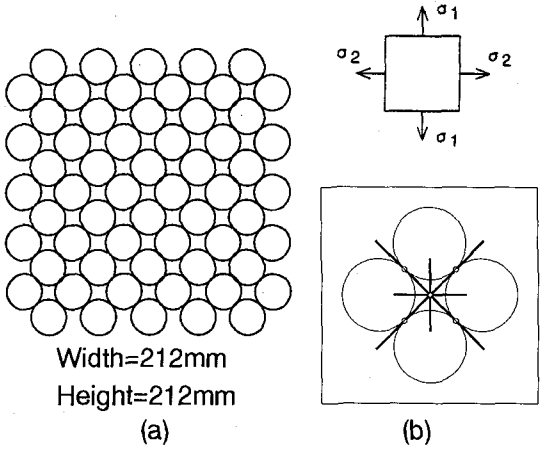

Figure 6 Numerical Concrete Specimen
(a) Element Allocation ; (b) Contact Lines

Numerical simulations are made to study the behavior of concrete specimen ($200 \times 200mm$) used by Kupfer et al.[7] under compression, tension and combined compression and tension. The numerical concrete specimen is shown in Fig.6 consisting of 60 elements of radius $R = 15mm$. The diagonal angle between elements is chosen to be 45 degrees to make the specimen symmetric in the vertical and horizontal directions. The element size and the element allocation are chosen so as to give sufficient accuracy for the deformational behavior under biaxial loading. The constraint between the concrete and the horizontal and vertical loading plates is assumed negligible. The material constants used are summarized in Appendix A. Those material constants and other parameters are identified through numerical simulations by comparing with the experimental data. The material properties are assumed uniform in the present study.

6.1 Simulation of behavior under compression

Numerical simulations are made to investigate the behavior of concrete specimen under uniaxial and biaxial compression for different stress ratios.

Fig.7 shows the simulation results of concrete under uniaxial compressive loading. A symbol with a prime indicates a quantity related to compression. It can be noticed from Fig.7(a) that the stress-strain curve obtained by numerical simulation has a good agreement with the experimental result and can continue through the softening behavior. The volume change process under compressive stress is simulated as shown in Fig.7(b). The simulation result indicates that the volume expansion due to cracking starts earlier than the experimental result. The reason is presumably that the present model is easy to expand laterally forming vertical cracks as shown in the final crack pattern in Fig.7(c). After vertical cracking diagonal cracks occur near the global failure. The final deformation pattern in Fig.7(d) indicates that excessive expansion occurs horizontally due to the vertical cracks.

Fig.8 shows the simulation results of concrete under biaxial compressive loading for $\sigma_2/\sigma_1 = 0.52$ where σ_1 is the applied vertical stress while σ_2 is the applied horizontal one. As shown in Fig.8(a) the stress-strain curve has a good agreement with the experimental result up to the peak and also can continue through the softening behavior up to the global failure. The final crack pattern shown in Fig.8(b) indicates that the global failure occurs due to the crushing near the top and bottom surface of the specimen with vertical tensile cracks near those surfaces. The final deformation pattern shown in Fig.8(c) indicates that the crushing occurs at the top and bottom row elements.

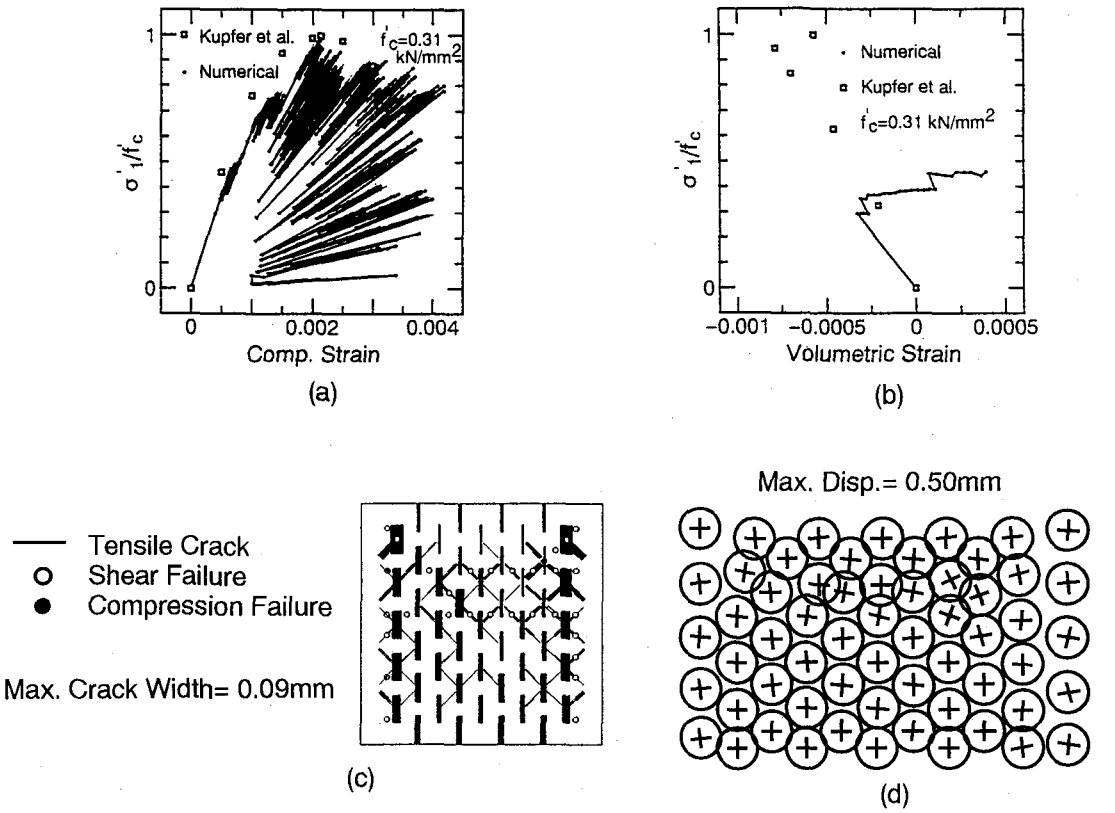

Figure 7 Simulation of Concrete Specimen under Uniaxial Compression
(a) Stress-Strain Realtionship ; (b) Volume Change Process ;
(c) Final Crack Pattern ; (d) Final Deformation Pattern

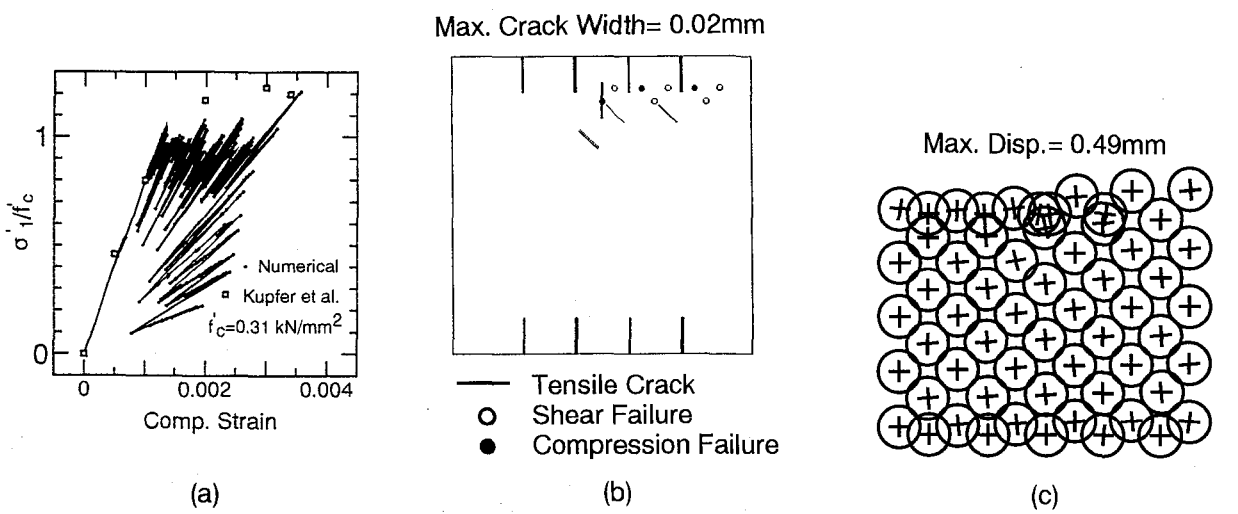

Figure 8 Simulation of Concrete Specimen under Biaxial Compression ($\sigma_2/\sigma_1 = 0.52$)
(a) Stress-Strain Relationship ; (b) Final Crack Pattern ; (c) Final Deformation Pattern

Fig.9 shows the simulation results of the concrete specimen under biaxial compressive loading for $\sigma_2/\sigma_1 = 1.0$. The stress-strain curve obtained by numerical simulation shown in Fig.9(a) indicates that the simulation peak strain is less than the experimental one. The final crack pattern shown in Fig.9(b) indicates that the global failure occurs due to the crushing near the bottom surface of the specimen with vertical cracks between the bottom row elements. The final deformation pattern in Fig.9(c) indicates that the crushing occurs at the bottom row elements.

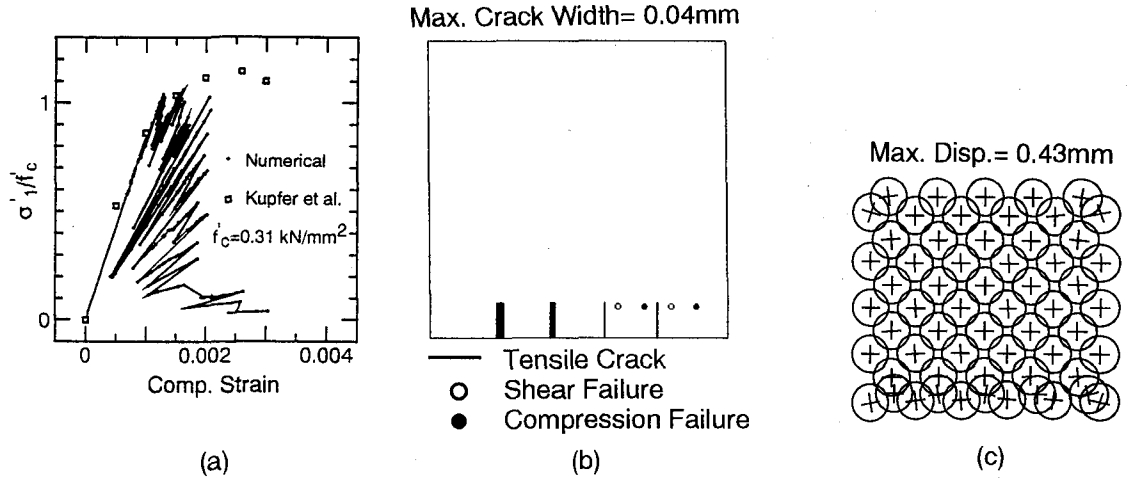

Figure 9 Simulation of Concrete Specimen under Biaxial Compression ($\sigma_2/\sigma_1 = 1.0$)
(a) Stress-Strain Relationship ; (b) Final Crack Pattern ; (c) Final Deformation Pattern

6.2 Simulation of behavior under tension

Numerical simulations are made to investigate the behavior of concrete specimen under uniaxial and biaxial tension for different stress ratios.

Fig.10 shows the simulation results of concrete specimen under uniaxial tensile loading. It can be noticed from Fig.10(a) that the simulation stress-strain curve has a good agreement with the experimental one including the gradual softening up to the global failure. The final crack pattern shown in Fig.10(b) indicates that the global failure is due to the horizontal tensile crack associated with local shear failure which occurs in the middle of the specimen. The final deformation pattern in Fig.10(c) shows the separation occurring in the specimen due to cracking.

Fig.11 shows the simulation results of the concrete specimen under biaxial tensile loading for $\sigma_2/\sigma_1 = 0.52$. As shown in Fig.11(a) the stress-strain curve obtained by numerical simulation has a good agreement with the experimental result up to the peak. The post-peak behavior is also simulated with gradual softening. The final crack pattern shown in Fig.11(b) indicates that the global failure is due to the horizontal tensile cracks which occur near the top surface of the specimen. The top cracks are linked together with local diagonal cracks to form a continuous crack. The final deformation pattern shown in Fig.11(c) indicates the separation of the top row elements from the specimen.

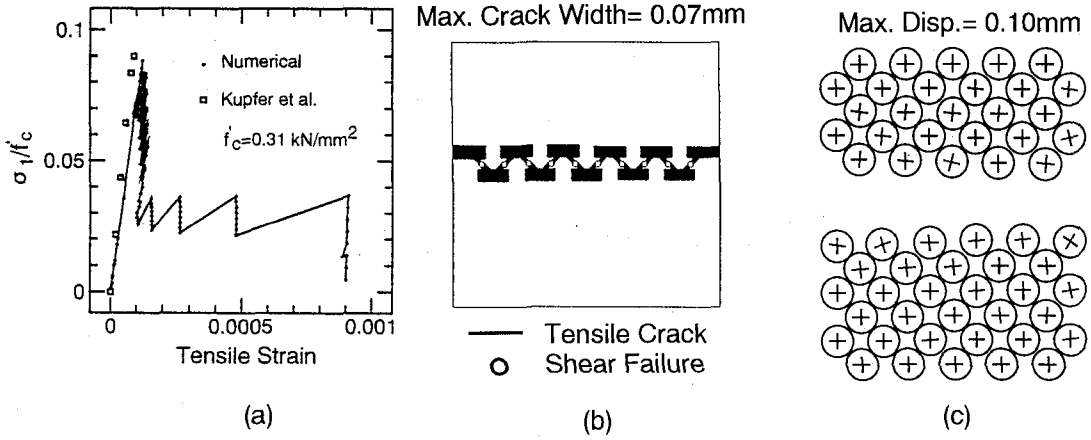

Figure 10 Simulation of Concrete Specimen under Uniaxial Tension
(a) Stress-Strain Relationship ; (b) Final Crack Pattern ; (c) Final Deformation Pattern

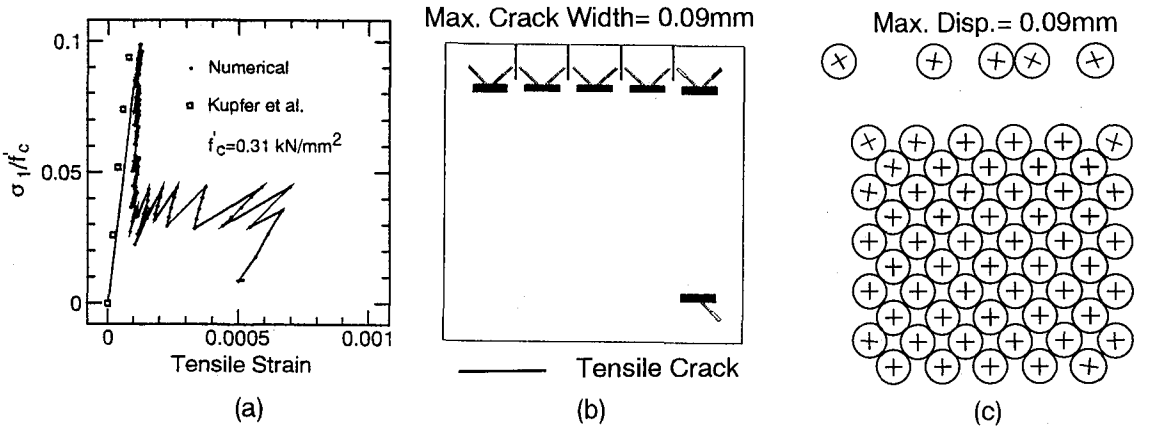

Figure 11 Simulation of Concrete Specimen under Biaxial Tension ($\sigma_2/\sigma_1 = 0.52$)
(a) Stress-Strain Relationship ; (b) Final Crack Pattern ; (c) Final Deformation Pattern

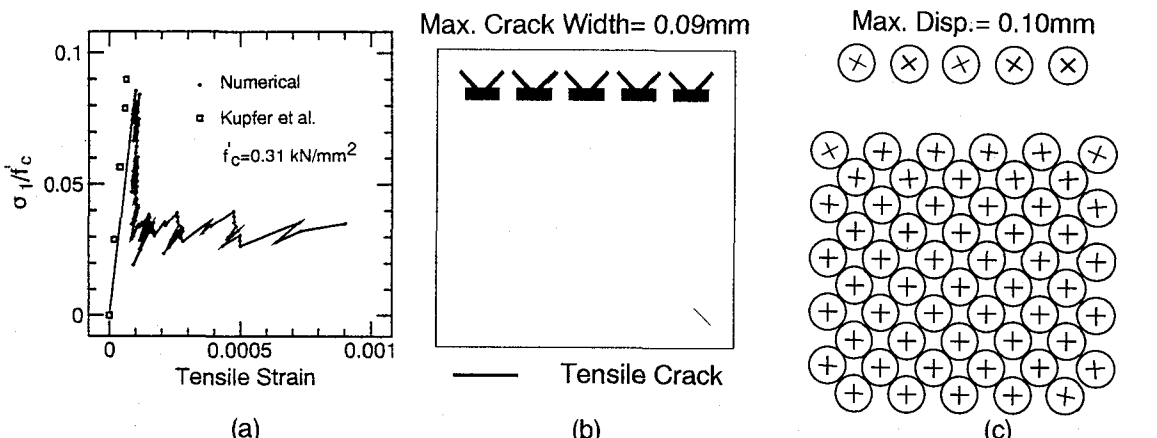

Figure 12 Simulation of Concrete Specimen under Biaxial Tension ($\sigma_2/\sigma_1 = 1.0$)
(a) Stress-Strain Relationship ; (b) Final Crack Pattern ; (c) Final Deformation Pattern

Fig.12 shows the simulation results of the concrete specimen under biaxial tensile loading for $\sigma_2/\sigma_1 = 1.0$. The stress-strain curve shown in Fig.12(a) has a good agreement with the experimental one up to the global failure. The final crack pattern shown in Fig.12(b) indicates that the global failure is due to the tensile cracks near the top surface of the specimen. The final deformation pattern is shown in Fig.12(c) indicating the separation occurring at the top row elements of the specimen.

6.3 Simulation of behavior under combined compression and tension

Numerical simulations are made to investigate the behavior of concrete specimen under combined compression and tension for different stress ratios.

Fig.13 shows the simulation results of the concrete specimen for $\sigma_2/\sigma_1 = -0.204$ where σ_1 is the vertical applied compressive stress and σ_2 is the horizontal applied tensile stress. It is noticed from Fig.13(a) that the simulation stress-strain curve has a good agreement with the experimental one and can describe the softening behavior up to the global failure. The final crack pattern shown in Fig.13(b) indicates that the global failure is due to the vertical tensile cracks occurring in the specimen. The final deformation pattern indicates the crushing in the specimen.

6.4 Failure envelope

The failure envelope of the concrete specimen under biaxial stresses is made using the simulation results and compared with the experimental one by Kupfer[7]. The strength of the numerical concrete specimen is determined by the maximum stress point of the stress-strain curve for each loading case. It can be noticed from Fig.14 that a good agreement is obtained between the simulation failure envelope and the experimental one.

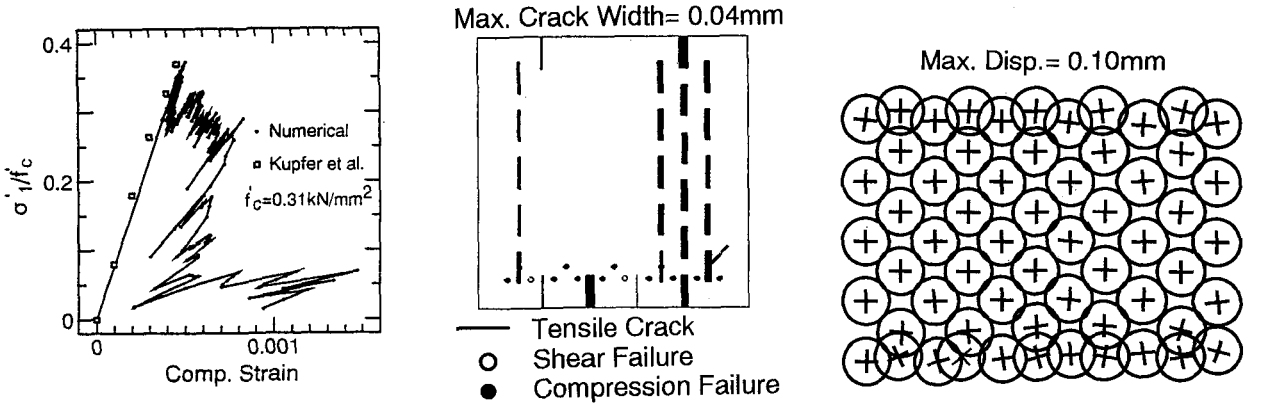

(a) (b) (c)

Figure 13 Simulation of Concrete Specimen under Combined Compression and Tension ($\sigma_2/\sigma_1 = -0.204$)
(a) Stress-Strain Relationship ; (b) Final Crack Pattern ; (c) Final Deformation Pattern

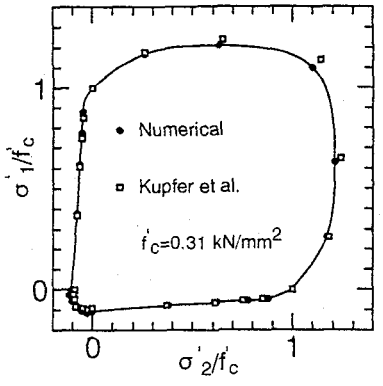

Figure 14 Failure Surface Envelope of Numerical Concrete Specimen

7. CONCLUSIONS

Through numerical simulations, it is confirmed that the disk element model is able to simulate the macroscopic stress-strain relationship and the failure behavior of concrete under biaxial compression, tension, and combined compression and tension. The internal crack formation up to the global failure is obtained through the present numerical model. Hence, the appropriateness of the assumed mesoscopic material models is confirmed. More accurate simulation is possible by extending the present method to the incremental method with iteration procedure.

Appendix A CONSTANTS USED IN SIMULATION

The material constants and other parameters used in the simulation are summarized as follows:

1. Elastic modulus $E^c = 12kN/mm^2$
2. Shear regidity $G^c = 5kN/mm^2$
3. Tensile strength $\sigma_n^t = 0.021kN/mm^2$
4. Comp. strength $\sigma_n^c = 0.21kN/mm^2$
5. Shear strength $\sigma_t^o = 0.021kN/mm^2$
6. Gradual degradation number for compression stiffness $n_d = 2$
7. Gradual degradation number for shear stiffness $n_d = 4$
8. Number of contact line layers $n_l = 5$

REFERENCES

1) Cundall, P.A.: A computer model for simulating progressive large-scale movements in blocky rock systems, *Proc. Symp. Int. Soc. Rock Mech.*, Nancy, 2, No.8, 1971.
2) Cundall, P.A. and Strack, O.D.L.: A discrete numerical model for granular assemblies, *Géotechnique*, Vol.29, No.1, pp.47–65, 1979.
3) Zubelewicz, A. and Bažant, Z.P.: Interface element modeling of fracture in aggregate composites, *J. Eng. Mech., ASCE*, Vol.113, No.11, pp.1619–1630, 1987.
4) Schlangen, E. and Mier, J.G.M.: Simple lattice model for numerical simulation of fracture of concrete materials and structures, *Materials and Structures*, No.25, pp.534–542, 1992.
5) Tsubaki, T.: Numerical simulation of deformational properties of concrete by using microstructural unit elements, *Proc. of the Japan Concrete Institute*, Vol.17, No.2, pp.1241–1246, 1995.
6) Vecchio, F.J. and Collins, M.P.: The modified compression field theory for reinforced concrete elements subjected to shear, *ACI J.*, Vol.83, No.2, pp.219–231, 1986.
7) Kupfer, H., Hilsdorf, H.K. and Rüsch, H.: Behavior of concrete under biaxial stresses, *ACI J.*, Vol.66, No.8, pp.656–666, 1969.

(Received September 18, 1995)